

# Electrohydrodynamic Printing-Based Heterointegration of Quantum Dots on Suspended Nanophotonic Cavities

Gregory G. Guymon, David Sharp, Theodore A. Cohen, Stephen L. Gibbs, Arnab Manna, Eden Tzanetopoulos, Daniel R. Gamelin, Arka Majumdar, and J. Devin MacKenzie\*

Nanophotonic structures are a foundation for the growing field of light-based quantum networks and devices enabled by their ability to couple with and manipulate photons. Colloidal quantum dots (QDs) are uniquely suited to complement this range of devices due to their solution-processability, broad tuneability, and near-unity photoluminescence quantum yields in some cases. To bridge the gap between them, electrohydrodynamic inkjet (EHDIJ) printing serves as a highly precise and scalable nanomanufacturing method for deterministic positioning and deposition of attoliter-scale QD droplets. This includes heterointegration in devices that are challenging to create by conventional subtractive semiconductor processing, such as QDs emitters coupled to substrate-decoupled nanoscale resonant structures. In this work, the first successful application of EHDIJ printing for the integration of these colloidal QDs into suspended nanophotonic cavities is demonstrated, achieving selective single-cavity deposition for cavity pairs as close as 100 nm apart. These results motivate the development of future suspended hetero-integrated devices that utilize EHDIJ printing as a sustainable, additive, and scalable method for quantum photonics nanomanufacturing.

single photon emissivity, and ligand-stabilized dispersity for solution processing.<sup>[3–6]</sup> Furthermore, the ability to tune the emission wavelength peak of the quantum dots by adjusting their size and chemistry offers them the flexibility to couple with a broad range of photonic platforms.<sup>[7]</sup> The utility of colloidal QD emitters can be further extended via hetero-integration with photonic cavities that maximize the emitter's emission intensity via the Purcell Effect, narrow its linewidth, and enable novel effects such as on-chip lasing and low-power optical nonlinearity.<sup>[8,9]</sup>

Silicon nitride ( $\text{Si}_3\text{N}_4$ ) has emerged as one leading material candidate for visible wavelength nanophotonic structures owing to its broad transparency window, Si CMOS compatibility, high visible refractive index, and low loss. For example, waveguides with ultralow loss and ring resonators with ultrahigh quality factors utilizing  $\text{Si}_3\text{N}_4$  have been demonstrated.<sup>[10,11]</sup> 1D photonic crystal nanobeam cavities represent an attractive geometry because their inherently small mode volumes maximize the light-matter coupling with hetero-integrated QDs at visible wavelengths. However, the low refractive index of  $\text{Si}_3\text{N}_4$  ( $n \approx 2$ ) limits the optical bandgap size and thus quality factor and mode confinement attainable in a high index local environment. To overcome these limitations and achieve higher Q-factors, researchers

## 1. Introduction

Colloidal quantum dots (QDs) have recently been at the forefront of research in hybrid integrated large-area and photonic devices for applications ranging from consumer information displays to quantum optical devices, computing, and sensors.<sup>[1,2]</sup> Semiconductor quantum dots are of considerable interest for these applications due to their, in some cases, near-unity quantum yields,

G. G. Guymon, J. D. MacKenzie  
Mechanical Engineering Department  
University of Washington  
Seattle, WA 98195, USA  
E-mail: [jdmacken@uw.edu](mailto:jdmacken@uw.edu)

D. Sharp, A. Manna, A. Majumdar  
Department of Physics  
University of Washington  
Seattle, WA 98195, USA

T. A. Cohen, D. R. Gamelin, A. Majumdar, J. D. MacKenzie  
Molecular Sciences and Engineering Institute  
University of Washington  
Seattle, WA 98195, USA

S. L. Gibbs, E. Tzanetopoulos, D. R. Gamelin  
Department of Chemistry  
University of Washington  
Seattle, WA 98195, USA

A. Majumdar  
Department of Electrical and Computer Engineering  
University of Washington  
Seattle, WA 98195, USA

J. D. MacKenzie  
Materials Science and Engineering Department  
University of Washington  
Seattle, WA 98195, USA

 The ORCID identification number(s) for the author(s) of this article can be found under <https://doi.org/10.1002/admt.202301921>

DOI: 10.1002/admt.202301921

have proposed suspended nanobeam cavities, as opposed to designs monolithically integrated onto the substrate.<sup>[12]</sup>

Laboratory-scale methods of integrating solution-processible QDs with these platforms have largely been confined to macroscale drop casting and spin coating, which typically deposits QDs with areal coverages with dimensions that are orders of magnitude greater than the intended target.<sup>[8,9]</sup> These processing techniques, however, have several drawbacks. First, they can result in very inefficient utilization of often toxic and environmentally concerning materials such as Cd and Pb and are inconsistent with large-scale, sustainable manufacturing. Drop casting and spin coating can also lead to residual QDs outside of the intended target area that may detrimentally affect the function of other parts of the system or cause an unwanted background emission or absorption that can mask the desired action of the device. Lastly, drop casting and spin coating techniques can put significant mechanical stresses on inherently fragile suspended nanophotonic structures due to capillary, kinetic, and thermal effects during the coating and drying stages of these processes. The materials waste and negative physical effects of these processes can be reduced by printing with conventional piezo-inkjet technology, which forms droplets >1 pL in volume and feature sizes >10 μm.<sup>[13]</sup> These dimensions, however, are still significantly larger than the often submicron feature sizes common in visible wavelength nanophotonic structures.<sup>[14]</sup> By utilizing subtractive processing, masks or templates, greater resolution and precision can be achieved. This, however, comes at the cost of design workarounds or concessions that must be made to accommodate the mask or template deposition and removal.

Alternatively, electrohydrodynamic inkjet (EHDIJ) printing has emerged over the past decade as an advanced manufacturing method for scalable contactless solution deposition with droplet sizes down to the attoliter scale.<sup>[15,16]</sup> EHDIJ printing is an electrophoretic additive manufacturing process that uses an applied electric field between the nozzle and target to selectively deposit charged materials down to nanoscale resolutions (~35 nm).<sup>[17]</sup> EHDIJ printing has been investigated for manufacturing circuitry interconnects,<sup>[18–20]</sup> flexible electronics,<sup>[21–24]</sup> photodetectors,<sup>[25–27]</sup> solar cell electrodes,<sup>[28–30]</sup> metasurfaces,<sup>[13,31]</sup> and light emitting diodes.<sup>[32–34]</sup> In regards to EHDIJ printing nanocrystals on nanophotonic structures, early work demonstrated an electrostatic autofocusing effect that could be utilized to selectively deposit onto edge-shaped geometries (such as waveguides and pillars) with enhanced efficacy.<sup>[17,35,36]</sup> Recently, Cohen et al. applied these mechanisms to demonstrate EHDIJ printing of lead-halide perovskite nanocrystals onto monolithic nanophotonic cavities.<sup>[37]</sup> This work was supported with additional analysis to confirm the negligible effects of applied electric fields on the structure and performance of the QDs, thus demonstrating their strong compatibility with the EHDIJ printing process.

Herein, we address the challenges of hybrid integration for high-performance suspended nanophotonic structures through the use of contactless electrohydrodynamic inkjet printing. We utilize robust CdSe/CdS core-shell QDs as photoactive materials, prepared in a cosolvent ink designed for the EHDIJ printing process. The materials are integrated into dielectric-mode silicon nitride-suspended cavity pairs, designed to photonically couple with the peak emission wavelength of the QDs, at varying cavity

separation distances. This work demonstrates the first, and only known, method for the deterministic positioning of quantum dots onto suspended photonic structures, with nanoscale precision.

## 2. Results and Discussion

CdSe quantum dots were synthesized via a modified hot injection colloidal synthetic approach.<sup>[38]</sup> To improve their photoluminescence quantum yield (PLQY), a CdS shell was grown over the core CdSe by slow-injection of cadmium oleate and octanethiol.<sup>[4]</sup> To prepare the synthesized core/shell QDs as a stable colloidal ink for printing, the particles were dispersed in a 1:1 octane:hexadecane mixture to a suitable concentration, indicated by the optical density of the first excitonic absorption peak (see Figure S1, Supporting Information). Figure 1a shows the normalized absorption and photoluminescence (PL) of the stabilized colloidal QD ink, with peak PL centered ~624 nm. The inset images in Figure 1a shows a colloidal QD ink under ambient light illumination (left) and UV illumination (right). The lack of sub-bandgap scattering in the absorption spectrum and the lack of haziness in the left image showcase the high colloidal stability of the QD ink. The rich, scarlet fluorescence in the right image demonstrates the strong fluorescence of the QDs in this EHDIJ ink. Figure S2 (Supporting Information) shows a TEM image of a drop cast and dried QD ink to provide a closer look at the shapes and sizes of these QDs. The QDs are spherical in shape with an average diameter of  $6.1 \pm 0.8$  nm.

Silicon nitride nanobeams were fabricated using standard nanofabrication techniques based on Si<sub>3</sub>N<sub>4</sub> thin films on Si substrates (see Experimental Section). After lithography and etching, this process yields an array of silicon nitride nanobeams that are air-surrounded (below, to the sides, and between the waveguides), with the exception of connection of the beams to the substrate only at their fixed ends. Nanobeams were fabricated in pairs, with beam separation distances ranging from 100 to 500 nm. To determine the photoluminescent coupling and resonance of the QDs and the cavities, the devices were illuminated with 445 nm continuous wave excitation and measured via their PL spectrum. The observed peak of the spectrum indicates the resonance of the cavities. The device's quality factor (Q) can be calculated according to:

$$Q = \frac{\lambda_0}{\Delta\lambda} \quad (1)$$

where  $\lambda_0$  and  $\Delta\lambda$  are the resonant wavelength and linewidth, respectively, of the cavity mode's Lorentzian line shape.

Q is a useful indicator for describing the overall spectral purity, efficiency of the emission, and coupling strength of a hetero-integrated system. Higher quality factors can be associated with high spectral purity, relatively low loss, and strong light-matter coupling with emitters. Figure 1b shows the PL spectrum of a nanobeam with 500 nm separation distance, fit with a Lorentzian curve, revealing a quality factor of ~3400. Beams with a 500 nm separation distance can each be treated as completely isolated nanophotonic structures, demonstrated by the single sharp resonance peak at ~625 nm. However, reducing the separation distance of the beams to 100 nm yields sufficient inter-cavity

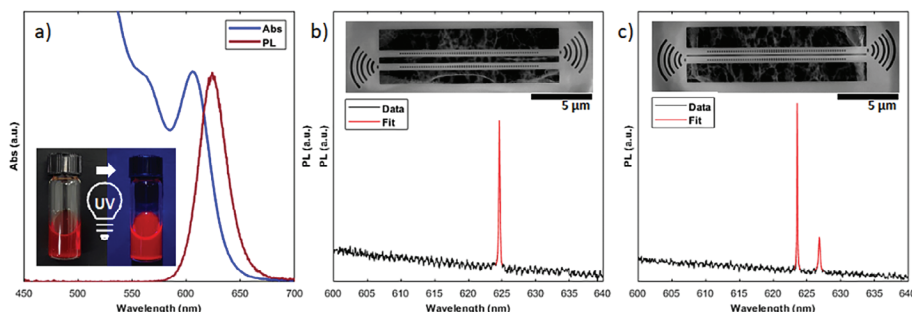


**Figure 1.** a) Normalized absorption and PL spectra of CdSe/CdS quantum dots. Inset: Image comparison of the colloidal QD ink under ambient and ultra-violet (UV) lighting conditions. b) PL characterization of 500 nm separated suspended  $\text{Si}_3\text{N}_4$  cavity. Inset: SEM imagery of the respective fabricated device. The presence of a single mode peak at  $\sim 625$  nm indicates no coupling at this distance. c) PL characterization of 100 nm separated suspended  $\text{Si}_3\text{N}_4$  cavity. The two peaks between 620 nm and 630 nm are assigned to two cavity supermodes, which indicates that these cavities are strongly coupled at this distance. Inset: SEM micrographs of the respective fabricated devices.

electric-field overlap to enter a strongly coupled regime, as seen by the two peaks in Figure 1c, with Q factors of  $\approx 5400$  and  $\approx 2360$  for supermodes 1 and 2, respectively. This result confirms the functionality of this device's architecture for investigating the spatial influence of photonic cavities, prior to the hetero-integration of photoactive materials. Inset images of Figures 1b,c highlight the cavity's suspended design, with a distinct trench etched from around and below the beams. Each device was fabricated with wedge-shaped concentric gratings to the right of the top waveguide and to the left of the bottom waveguide. These gratings diffuse light from either beam after hetero-integration and indicate the presence or absence of coupling. The web-like substance below the beams is a residual byproduct of the isotropic  $\text{XeF}_2$  etching process.

The colloidal quantum dots were physically integrated with the nanophotonic cavities via high-resolution electrohydrody-

namic inkjet (EHDI) printing. Figure 2 shows a schematic of the EHDI tool used for this work. Colloidal inks were pipetted into pulled borosilicate glass capillary printheads that were then magnetically mounted to an electrode on the tool. Next, the substrate containing the suspended cavity pairs were secured to a grounded printing stage via a vacuum chuck. The parameters for printing were determined by finding the minimum voltage threshold for steady-state droplet ejection on a non-etched portion of the device's substrate. The parameters were further optimized for printing on the suspended cavities by raising the minimum voltage threshold enough to prevent destabilization of the steady-state ejections, caused by the fluctuating strength of the electric field as the printhead passes over the trench of the device. The minimum voltage threshold can be raised by increasing the voltage bias above the minimum for ejection. Printing was initiated using a 75% square-wave alternating current (AC) that is

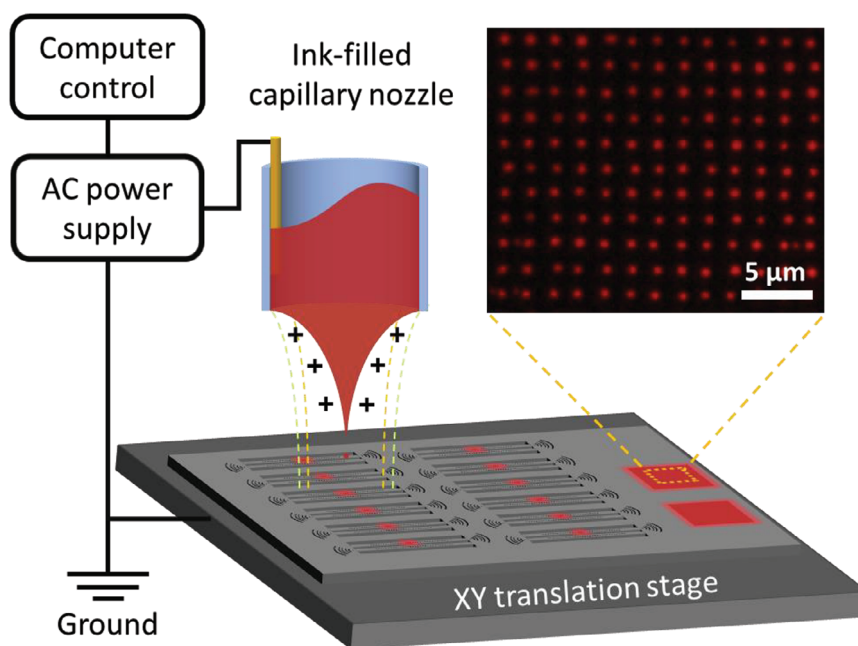


**Figure 2.** Schematic of the electrohydrodynamic inkjet printing setup used in this work. The inset image shows PL microscopy with 450 nm excitation of CdSe/CdS quantum dots printed with  $2 \mu\text{m}$  pitch.

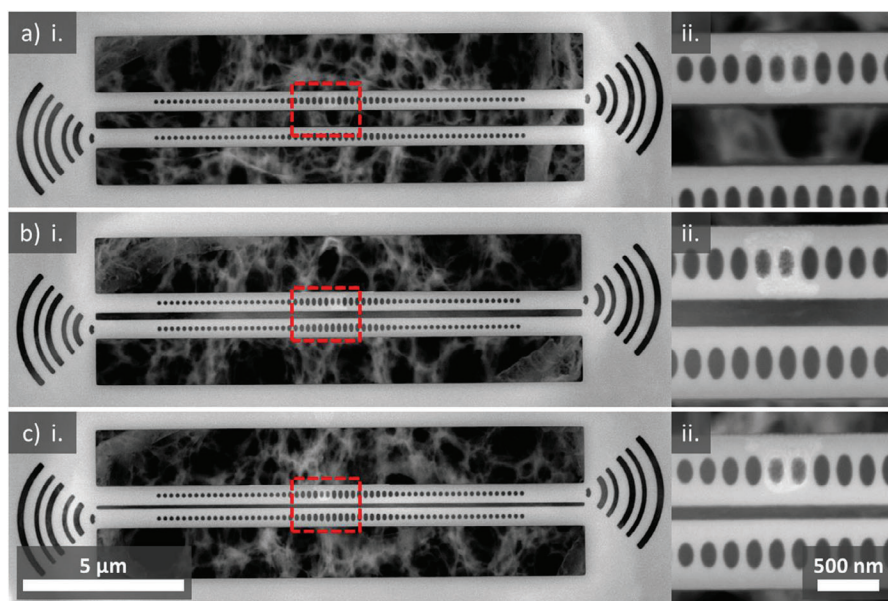


**Figure 3.** SEM imagery of suspended cavity beam pairs post-EHDIJ printing. The micrographs show an aggregation of CdSe/CdS printed on a single beam for each pair. a) 500 nm beam separation. i. Device overview image. ii. Cavity print site image. b) 200 nm beam separation. i. Device overview image. ii. Cavity print site image. c) 100 nm beam separation. i. Device overview image. ii. Cavity print site image.

activated over the pre-determined deposition sites with a bias of 230 V, an amplitude of 50 V, and a frequency of 1 kHz. In principle, the bias polarizes the particles in the solution to overcome the surface energetics that limit droplet sizes in conventional inkjet printing and stabilizes a surface-charged convex meniscus at the tip of the printhead. The amplitude is then applied at the given frequency to overcome the surface energy of the meniscus, forming a Taylor cone that extends along the direction of the electric field. Next, hydrostatic destabilization of the tip of the Taylor cone causes droplets to form, which separate from the extended cone and are guided by the electric field toward to stage. The ejected droplet's final position is determined by the planar movement of the step-motor-driven translation stage that can move the substrate stage with 100 nm step sizes and no hysteresis. To align the printhead's deposition site to the cavity target, the printer utilizes a two-stage alignment process. The first stage determines the position and orientation of the substrate by positioning the alignment camera to calibration features on the substrate. The second stage determines the position of the printhead's nozzle by calibrating the alignment camera to an initial printing test feature. The two-stage alignment process adapts the local coordinates of the printing design by including any offset or rotation required by the position and orientation of the substrate or nozzle, relative to the stage's global coordinates. An example of the printing precision that can be achieved with this tool is demonstrated in the microscopy image of a printed CdSe/CdS QD array in Figure 2. Measuring the volume of as-printed QD deposits with atomic force microscopy yielded a mean of  $\approx 3.34 \pm 0.86$  attoliters per print (Figure S3, Supporting Information). By modulating the strength of the electric field, for the micron-scale inner diameter nozzles used here, prints ranging from sub-pico to attoliter-scale volumes can be expected.

The SEM images in Figure 3 shows a series of dielectric-mode  $\text{Si}_3\text{N}_4$  cavities after alignment to structures on the device sub-

strate and CdSe/CdS QD printing. Here, the presence of QDs solely on the upper beam indicates that the printed droplet only contacts and deposits QDs onto a single cavity from each pair down to cavity spacings as small as 100 nm. Close examination of the suspended cavity print sites reveals that QDs appear to be wetting the center elliptical holes, but we note a lack of QDs observable at the edge of the elliptical cavity holes near the edges of the printed QD features. This behavior is likely explained by morphologically-induced reductions in surface energy and wetting compared to unpatterned  $\text{Si}_3\text{N}_4$ , such as in Cassie-Baxter wetting states or what is sometimes referred to as “the lotus effect”, where the surface energy cost of wetting a more complex and effectively higher surface area geometry prevents the penetration of the QD-ink.<sup>[39]</sup>

Following the electrohydrodynamic inkjet printing of the QDs, the asymmetric QD-coupled nanobeam pair devices were inspected using a PL microscope under 450 nm excitation. The microscopy in Figure 4a–c shows suspended cavity pairs with waveguide spacings of 500, 200, and 100 nm, respectively. The emissions from the cavity and waveguide coupled to the gratings at the edge of each waveguide. These gratings were used purely for qualitative microscopy measurements because their design allowed photonic coupling to be gauged by their relative brightness. In Figure 4a, the emissions from the right grating indicate strong coupling between the cavity and the quantum dots. The lack of emission from the left grating indicates no inter-cavity coupling for this waveguide's separation distance. The emission visible at the top of the left grating is due to its proximity to the top waveguide, which causes minor unintended grating coupling, but does not impact the performance of the device in any meaningful way. For the 200 nm separated cavity pair (Figure 4b), the brightness of the right grating indicates strong coupling between the QDs and the cavity, while the brightness of the left grating indicates detectable inter-coupling. The high light intensity at

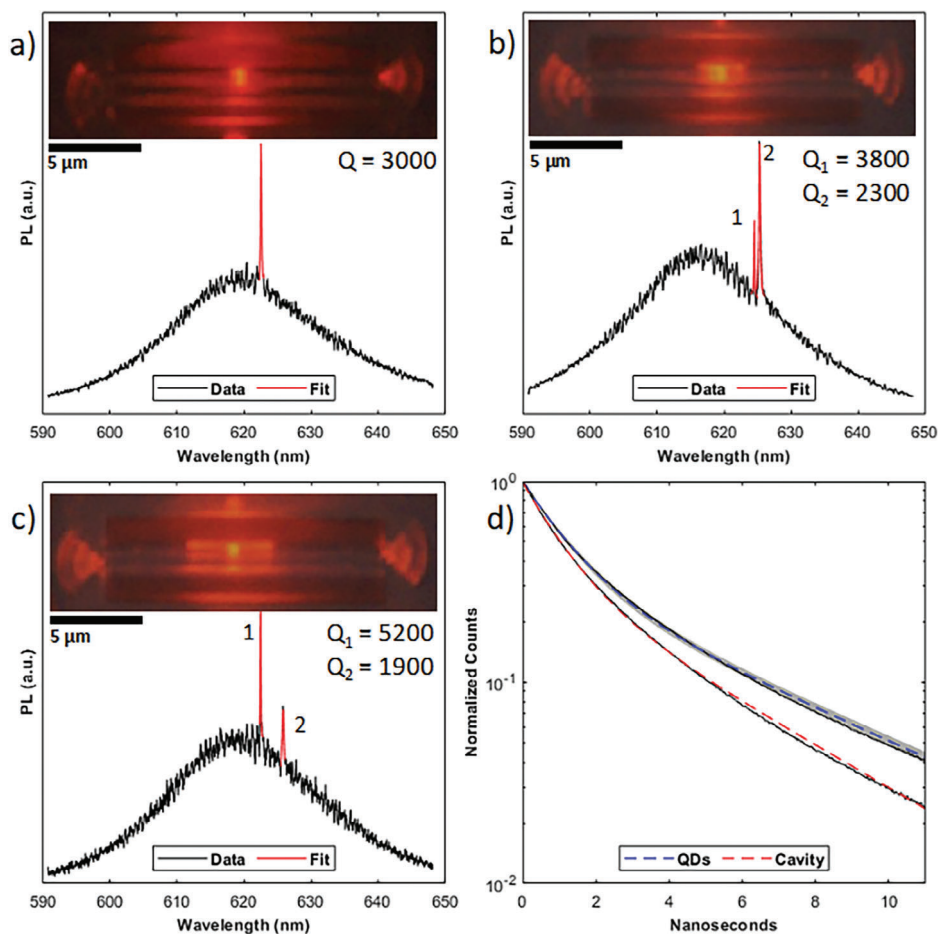


**Figure 4.** PL microscopy and characterization of asymmetrically printed QD-coupled suspended cavity pairs. a) PL spectra of 500 nm separated suspended nanobeam cavities. Inset: PL imagery of the respective cavity. b) PL spectra of 200 nm separated suspended cavities. Inset: PL imagery of the respective cavities. c) PL spectra of 100 nm separated suspended cavity. Inset: PL imagery of the respective cavity. d) PL lifetime measurements of QDs printed on the cavity site and outside of the cavity. The QD's dashed blue line represents the best-fit biexponential to the mean of the raw data (black) for the external QDs, accompanied by a shaded curve (gray) to represent the standard deviation of the fit. The cavity's dashed red line represents the fitted biexponential curve of the data (black) for the cavity-coupled QDs.

both gratings (Figure 4c) indicates that nanobeams separated by 100 nm show the strongest inter-cavity coupling.

Having identified the photonic coupling types present and their respective strengths in each suspended cavity design through qualitative PL microscopy, we further characterized these devices through quantitative spectroscopy methods. See the Experimental Section for the methodology of the PL characterization of these devices. Figure 4a shows PL spectra obtained by exciting the QDs with 532 nm light and collecting the resulting cavity emission from the right end of the top grating for asymmetrically printed QD-coupled nanobeam cavities separated by 500 nm. The broad peak is assigned to non-cavity coupled emission from the QDs, and the sharp peak at  $\approx 622$  nm is assigned to QD PL that is coupled to the fundamental mode of a single nanobeam cavity. We fit the sharp peak with a Lorentzian curve to obtain a quality factor of  $\approx 3000$ , with no other statistically significant peaks that would indicate inter-cavity coupling. As the cavity spacing is reduced to 200 nm, two sharp peaks become visible in the PL spectra shown in Figure 4b with a peak spacing of  $\approx 0.2$  Å. These two peaks, or supermodes, have different quality

factors ( $Q_1 \approx 3800$ ,  $Q_2 \approx 2300$ ) due to unintentional cavity fabrication variations, which leads to spectral detuning. When the supermodes are coupled, their behavior is interdependent and new eigenmodes are created that are the combination of the original modes. When these modes experience spectral detuning, meaning their respective frequencies differ slightly, their new eigenmodes differ as well. This results in offset quality factors that approximately average out to that of the isolated QD-cavity system (Figure 4d). In the case of these coupled supermodes, the original mode ( $Q_2$ ) is slightly red-shifted while the coupled mode ( $Q_1$ ) is blue-shifted in proportion to the inter-cavity spacing. To demonstrate this proportionality, Figure 4c shows the spectroscopy of the as-printed inter-cavity coupled device with a cavity spacing of 100 nm. Here, the separation of the supermodes ( $Q_1 \approx 5200$ ,  $Q_2 \approx 1900$ ) is increased to 3.4 nm, which corresponds to a stronger coupling strength. This behavior is in good agreement with previous work using CdSe/CdS QDs and monolithic silicon nitride nanobeam cavities.<sup>40]</sup>

Figure 4d shows QD PL lifetime data collected from the upper cavity of Figure 4a compared to data collected for the same

QDs that were printed away from the cavity. Because of the relatively large beam separation (500 nm), this system can be effectively treated as an isolated cavity for determining the Purcell enhancement of the hetero-integrated device. In both cases, the PL lifetimes were fitted to a biexponential decay. For the QDs that were not coupled to any cavities, the average fast and slow PL decay was  $1.18 \pm 0.07$  and  $5.31 \pm 0.17$  ns, respectively, whereas, for the cavity-coupled QDs, the fast and slow PL decay was 1.02 and 4.13 ns, respectively. This result corresponds to average Purcell factors of 1.15 and 1.29 for the fast and slow decay, respectively, which is in line with similar reports.<sup>[40]</sup> When compared to the maximum possible Purcell enhancement factor determined by finite-difference time-domain simulation (FDTD), the experimentally measured values were in good agreement with the simulated value of 1.34. Additional information about these calculations and data can be found in Section S3 (Supporting Information).

Colloidal quantum optical materials hetero-integrated with suspended photonic devices have been explored for their potential in next-generation optical devices, but no scalable, fully additive, and sustainable method exists to deterministically place these materials on such fragile nanostructures. By successfully combining CdSe/CdS core-shell QDs with these suspended silicon nitride nanobeam cavities in this work with EHDIJ printing, we convincingly demonstrate that this printing method has great potential to help elucidate the fundamental understanding of light-matter interactions and provide a viable path to manufacture fully integrated quantum photonic devices of unlimited scale and complexity. We show that the printing process has a minimal impact on emitter properties or cavity performance, and the patterning precision can reach length scales as small as 100 nm. To the best of our knowledge, this is the first demonstration of selective colloidal material positioning on suspended cavities at the length scales needed to demonstrate tunable inter-cavity coupling. Such fine patterning fidelity on these suspended structures could unlock the full potential of high gain nanomaterials,<sup>[41–44]</sup> magneto-optical nanoparticles,<sup>[45–47]</sup> and other narrow-linewidth emitters<sup>[48,49]</sup> with high Q-factor individual cavities,<sup>[12]</sup> cavity pairs,<sup>[50]</sup> and strain-tunable nanostructures.<sup>[51]</sup> These advanced hetero-integrated systems could be used to produce PT-symmetry lasers,<sup>[52,53]</sup> fully-integrated nanoscale optical networks,<sup>[54]</sup> and other unique device architectures that could not be fabricated without the methods described here. Furthermore, previous demonstrations of single emitter positioning with EHDIJ printing<sup>[36,55]</sup> and high-yield single-particle placement of individual silica-shelled CdSe/CdS QDs<sup>[49]</sup> suggest that this printing process could enable high-yield and high-precision patterning of individual emitters on nanophotonic devices to enable the manufacturing of single photon emitter-based integrated circuits.

Furthermore, the ability to deterministically deposit colloidal QDs onto air-clad photonic structures, with nanoscale precision, has yielded immediate improvements in coupling strength when compared to previous work on polymer-clad photonic cavities, as evident from our higher Purcell enhancement.<sup>[40]</sup> This opens the gates for new hybrid integrated device architectures that were previously considered impossible from a materials integration standpoint. For instance, recent work on in-situ strain tunable

suspended cavities shows the potential that EHDIJ printing could have for integrating a broad range of colloidal emitters into actively tunable photonic devices.<sup>[56]</sup>

Lastly, a significant contribution to the broad line widths of the as-printed QDs is due to the variation among emitters in an aggregate deposition. Seeking out reliable methods for deterministically positioning single QDs is becoming a focus for those interested in functionalizing colloidal emitters for their potential in single-photon manipulation and entanglement. Recent work has demonstrated the potential of giant oxide shells for singularly-positioned CdSe/CdS QDs, through capillary-driven self-assembly in substrates or removable templates.<sup>[49,57]</sup> Through ongoing optimization and reduction of QD counts, building on the work here, a path to a sustainable nanomanufacturing of single photon QD-based devices through additive hetero-integration using electrohydrodynamic inkjet printing is taking shape.

### 3. Conclusion

In conclusion, we have demonstrated the first additive hetero-integration method for directly patterning attoliter scale deposits of colloidal emitters selectively onto 3D free-space suspended nanophotonic cavities, spaced as close as 100 nm that exhibit inter-cavity coupling. As shown through high-resolution SEM imaging, electrohydrodynamic inkjet printing was able to preserve the physical integrity of the free-space 3D suspended nanobeam cavities, due to its inherently contactless process. Furthermore, PL characterization of the as-printed devices confirmed the suitability of EHDIJ printing for enabling supermode emissions from nanomanufactured QD-cavity and inter-cavity coupled nanobeams at nanoscale free-space separations. These results should encourage additional research into hetero-integrated suspended devices, as further improvements to emitter quality, cavity fabrication disorder, printhead size, and stage precision would all serve to enhance overall device quality. Addressing these problems on all fronts will require convergent developments in chemistry, physics, materials science, electrical, and mechanical engineering.

### 4. Experimental Section

**Materials:** Cadmium oxide (CdO, 99.9%, Sigma–Aldrich), Se powder (200 mesh, 99.99%, Alfa Aesar), 1-octadecene (ODE, 90% tech grade, Sigma–Aldrich), oleic acid (OLAC, 90% tech grade, Sigma Aldrich), tri-n-octylphosphine oxide (TOPO, 99%, Sigma Aldrich), hexadecylamine (HDA, Sigma Aldrich), trioctylphosphine (TOP, 97% Sigma–Aldrich), 1-octanethiol (99%, Sigma–Aldrich), toluene (certified ACS, Fisher Chemical), ethyl acetate (certified ACS, Fisher Chemical), octane (reagent grade, Sigma–Aldrich), n-hexadecane (99%, Sigma–Aldrich).

**Nanocrystal Synthesis and Solution Preparation:** CdSe QDs were synthesized according to a modified method from that previously reported.<sup>[38]</sup> 130 mg (1 mmol) CdO powder was loaded into a 100 mL 3-neck reactor along with 16 g ODE and 0.6 g OLAC. This mixture was placed under vacuum at 110 °C for 45 min. Then it was placed under N<sub>2</sub> flow, heated to 290 °C, and kept there for 5 min. The red mixture should turn clear as Cd-oleate forms. The solution was allowed to cool to 100 °C when 2.0 g TOPO and 1.8 g HDA (both solids) were added into the reactor. The reactor was placed under vacuum at 110 °C for 15 min, then placed under N<sub>2</sub> and heated to 290 °C. Once the temperature stabilized, a solution of 100 mg (1.3 mmol) Se dissolved in 2 mL TOP was swiftly injected. The

reaction proceeded for 2 min and was quenched via a water bath. The particles were washed 3 times with ethyl acetate and toluene.

The methodology for the CdS shelling process was derived from previously reported work.<sup>[4]</sup> It requires the synthesis of Cd-oleate as a precursor. Cd-oleate at a concentration of 0.2 M in OLAC was prepared by mixing 1.28 g CdO in 31.5 mL OLAC and 18.3 mL ODE in a three-neck reactor. The mixture is degassed at 110 °C for 1 hr and then placed under N<sub>2</sub> and heated to 160 °C until Cd-oleate forms (≈30 min). The Cd-oleate was stored in an N<sub>2</sub> glovebox.

To grow the CdS shells, 100 nmol of CdSe QDs were dispersed in 6 mL of ODE in a three-neck reactor and degassed at 110 °C for 1 h. The mixture is heated to 310 °C. As the temperature increases, injection of two precursors begins when the temperature reaches 240 °C. 0.2 M Cd-oleate and 0.2 M 1-octanethiol in ODE were simultaneously injected at a rate of 0.05 mL min<sup>-1</sup>. Increased injection volume increases the CdS shell thickness. For these particles, the total injected volume of each precursor was 2.5 mL (45 min injection). The particles were washed 3x via ethanol and toluene.

Lastly, the colloidal printing inks were prepared according to a previously reported methodology.<sup>[37]</sup> CdSe/CdS core/shell quantum dots were prepared as an ink for printing by crashing a known quantity of dots from the stock solution. The crashed pellet was dispersed in 1:1 octane and hexadecane to a volume that puts the optical density of the first excitonic absorption peak at 0.8 in a 1 cm pathlength cuvette.

**Nanophotonic Cavity Design and Fabrication:** The Si<sub>3</sub>N<sub>4</sub> nanobeams were designed for operation in a suspended configuration. The waveguides use 200 nm thick Si<sub>3</sub>N<sub>4</sub> and are 15 μm long. For the dielectric-mode cavity design, the cavity region consisted of elliptical holes with a major radius of 132 nm, minor radius of 60 nm, and a fixed period of 195 nm. The defect was formed by quadratically tapering the major radii of these holes to 63 nm over the span of 15 periods. The waveguide width was fixed at 600 nm. An additional 20 elliptical holes on either side with the same major radii formed the Bragg mirror regions. According to finite-difference time-domain simulations (FDTD) (Lumerical, Inc), this resulted in a theoretical cavity quality factor of ≈20000 and a mode volume of ≈2 (( $\frac{a}{n}$ )<sup>3</sup>).

The Si<sub>3</sub>N<sub>4</sub> nanobeams were fabricated using 200 nm LPCVD Si<sub>3</sub>N<sub>4</sub> on a Si substrate. A 300 nm-thick ZEP520A electron beam lithography resist was spun-coat onto the chip, and electron-beam lithography followed by development in amyl acetate transferred the pattern to the resist. A plasma etch consisting of CHF<sub>3</sub>/O<sub>2</sub> chemistry transferred the pattern to the underlying SiN. After stripping the remaining resist with methylene chloride, an isotropic XeF<sub>2</sub> etch was used to etch the underlying Si and suspend the Si<sub>3</sub>N<sub>4</sub> nanobeams.

**Electrohydrodynamic Inkjet Printing:** Electrohydrodynamic inkjet printing was conducted by loading the prepared CdSe CdS<sup>-1</sup> ink into pulled borosilicate glass capillary pipettes with a tip internal nozzle diameter of 1–3 μm. These printheads were manufactured with an inlaid gold electrode along the interior wall of the pipettes that serves to apply a bias near the printing medium. After mounting the printhead into the printer and placing the substrate on a grounded stage vacuum chuck, an alignment process was used to map the designed printing patterns to the orientation of the target substrate. Upon completion, printing was initiated with the following parameters: Bias: 230 V, Amplitude: 50 V, Frequency: 1 kHz.

**Photoluminescence Characterization:** The Si<sub>3</sub>N<sub>4</sub> nanobeams were characterized using cavity-coupled PL both excited and collected directly from the centers of the nanobeams. All measurements were performed in a scanning PL microscopy set-up operating in ambient conditions. For the Si<sub>3</sub>N<sub>4</sub> nanobeams without CdSe/CdS QDs, a 445 nm continuous wave laser (CNI Laser MDL-III-445L) was focused on the center of the Si<sub>3</sub>N<sub>4</sub> nanobeam using a 100x/0.95 NA objective to excite PL from intrinsic Si<sub>3</sub>N<sub>4</sub> defects and excite the cavity mode. For Si<sub>3</sub>N<sub>4</sub> nanobeams with CdSe QDs, a 532 nm pulsed laser with a 10 MHz repetition rate (NKT SuperK FIAN-IUM) was focused on CdSe/CdS QD ink droplets positioned on the center of the nanobeams to measure the cavity mode coupled to CdSe/CdS QDs. The PL spectra were collected by detecting the PL with a Princeton Instruments Isoplone 160 spectrometer with a 1200 lines/mm grating coupled to a Pixis 400 CCD. Lifetime measurements were performed by detecting the PL of CdSe CdS<sup>-1</sup> QDs with avalanche photodiode single photon detec-

tors (Micro Photon Devices PDM) and synchronizing the detector signal with the pulsed laser repetition (PicoQuant TimeHarp 260). In all cases, a 550 nm LP (ThorLabs DMLP550) dichroic mirror in conjunction with a 550 nm LP filter (ThorLabs FEL0550) was used to filter out the pump laser.

## Supporting Information

Supporting Information is available from the Wiley Online Library or from the author.

## Acknowledgements

This work was primarily supported by the NSF Center for Integration of Modern Optoelectronic Materials on Demand (IMOD), an NSF Science and Technology Center, under grant agreement DMR-2019444 (to D.R.G., A.M., J.D.M.). Part of this work was conducted at the Molecular Analysis Facility, which is supported in part by funds from the Molecular Engineering & Sciences Institute, the Clean Energy Institute, and the National Science Foundation (NNCI-2025489 and NNCI-1542101). Part of this work was supported by the National Science Foundation (NSF) through the UW Molecular Engineering Materials Center, a Materials Research Science and Engineering Center (DMR-1719797 to D.R.G. and J.D.M.). Part of this work was also supported by the Washington Research Foundation (to A.M. and J.D.M.). Part of this work was supported by the Joint Center for Deployment and Research in Earth Abundant Materials (to J.D.M.). Part of this work was conducted at the Washington Clean Energy Testbeds, a facility operated by the University of Washington Clean Energy Institute.

## Conflict of Interest

The authors declare no conflict of interest.

## Data Availability Statement

The data that support the findings of this study are available from the corresponding author upon reasonable request.

## Keywords

electrohydrodynamic printing, hetero-integrated nanophotonics, quantum dots, scalable nanomanufacturing, suspended cavities

Received: November 13, 2023  
Revised: March 7, 2024  
Published online: March 30, 2024

- [1] J. Wang, F. Sciarrino, A. Laing, M. G. Thompson, *Nat. Photonics* **2020**, *14*, 273.
- [2] P.-Y. Hong, C.-H. Lin, I.-H. Wang, Y.-J. Chiu, B.-J. Lee, J.-C. Kao, C.-H. Huang, H.-C. Lin, T. George, P.-W. Li, *Appl. Phys. A* **2023**, *129*, 126.
- [3] A. B. Greytak, P. M. Allen, W. Liu, J. Zhao, E. R. Young, Z. Popović, B. J. Walker, D. G. Nocera, M. G. Bawendi, *Chem. Sci.* **2012**, *3*, 2028.
- [4] D. A. Hanifi, N. D. Bronstein, B. A. Koscher, Z. Nett, J. K. Swaback, K. Takano, A. M. Schwartzberg, L. Maserati, K. Vandewal, Y. van de Burgt, A. Salleo, A. P. Alivisatos, *Science* **2019**, *363*, 1199.
- [5] A. H. Proppe, D. B. Berkinsky, H. Zhu, T. Šverko, A. E. K. Kaplan, J. R. Horowitz, T. Kim, H. Chung, S. Jun, M. G. Bawendi, *Nat. Nanotechnol.* **2023**, *18*, 993.

- [6] B. A. Kairdolf, A. M. Smith, S. Nie, *J. Am. Chem. Soc.* **2008**, *130*, 12866.
- [7] L. Protesescu, S. Yakunin, M. I. Bodnarchuk, F. Krieg, R. Caputo, C. H. Hendon, R. X. Yang, A. Walsh, M. V. Kovalenko, *Nano Lett.* **2015**, *15*, 3692.
- [8] Z. Yang, M. Pelton, I. Fedin, D. V. Talapin, E. Waks, *Nat. Commun.* **2017**, *8*, 143.
- [9] S. Gupta, E. Waks, *Opt. Express* **2013**, *21*, 29612.
- [10] J. F. Bauters, M. J. R. Heck, D. D. John, J. S. Barton, C. M. Bruinink, A. Leinse, R. G. Heideman, D. J. Blumenthal, J. E. Bowers, *Opt. Express* **2011**, *19*, 24090.
- [11] E. S. Hosseini, S. Yegnanarayanan, A. H. Atabaki, M. Soltani, A. Adibi, *Opt. Express* **2009**, *17*, 14543.
- [12] M. Khan, T. Babinec, M. W. McCutcheon, P. Deotare, M. Lončar, *Opt. Lett.* **2011**, *36*, 421.
- [13] H. J. C. Brunner, J. Whitehead, R. Gibson, J. R. Hendrickson, A. Majumdar, J. D. MacKenzie, *Adv. Mater. Interfaces* **2022**, *9*, 2200149.
- [14] B. Derby, *Annu. Rev. Mater. Res.* **2010**, *40*, 395.
- [15] Y. Huang, F. Fang, F. Chen, X. Cui, J. Sun, D. Zhuang, J. Wei, *Nano Ex.* **2020**, *1*, 030008.
- [16] J. Schneider, P. Rohner, P. Galliker, S. N. Raja, Y. Pan, M. K. Tiwari, D. Poulikakos, *Nanoscale* **2015**, *7*, 9510.
- [17] P. Galliker, J. Schneider, H. Eghlidi, S. Kress, V. Sandoghdar, D. Poulikakos, *Nat. Commun.* **2012**, *3*, 890.
- [18] P. Rohner, A. Reiser, F. T. Rabouw, A. S. Sologubenko, D. J. Norris, R. Spolenak, D. Poulikakos, *Nanoscale* **2020**, *12*, 20158.
- [19] N. C. Schirmer, T. Schwamb, B. R. Burg, N. Hotz, D. Poulikakos, *Appl. Phys. Lett.* **2009**, *95*, 033111.
- [20] K. Rahman, A. Khan, N. M. Muhammad, J. Jo, K.-H. Choi, *J. Microelectromech. Syst.* **2012**, *22*, 065012.
- [21] P. Ren, J. Dong, *Adv. Mater. Technol.* **2021**, *6*, 2100280.
- [22] G. Kang, H. Lee, J. Moon, H.-S. Jang, D.-H. Cho, D. Byun, *ACS Appl. Nano Mater.* **2022**, *5*, 6726.
- [23] C. Nothnagle, J. R. Baptist, J. Sanford, W. H. Lee, D. O. Popa, M. B. J. Wijesundara, *Proc. SPIE* **2015**, *9494*, E3.
- [24] Y. Han, J. Dong, *Adv. Mater. Technol.* **2018**, *3*, 1700268.
- [25] Q. Wang, G. Zhang, H. Zhang, Y. Duan, Z. Yin, Y. A. Huang, *Adv. Funct. Mater.* **2021**, *31*, 2100857.
- [26] F. I. Alzackia, W. Jonhson, J. Ding, S. C. Tan, *ACS Appl. Mater. Interfaces* **2020**, *12*, 28840.
- [27] Q. Wang, G. Zhang, H. Zhang, Y. Duan, Y. A. Huang, in *Proceedings of the 16th Annual IEEE Int. Conf. on Nano/Micro Engineered and Molecular Systems*, IEEE, Xiamen, China, **2021**, pp. 652–655.
- [28] J.-A. Jeong, H.-K. Kim, J. Kim, *Sol. Energy Mater. Sol. Cells* **2014**, *125*, 113.
- [29] Y. Jang, I. Hartarto Tambunan, H. Tak, V. Dat Nguyen, T. Kang, D. Byun, *Appl. Phys. Lett.* **2013**, *102*, 123901.
- [30] D.-Y. Shin, J.-Y. Seo, H. Tak, D. Byun, *Sol. Energy Mater. Sol. Cells* **2015**, *136*, 148.
- [31] Y. Wu, Y. Deng, J. Wang, Z. Zong, X. Chen, W. Gu, *IEEE Trans. Terahertz Sci. Technol.* **2019**, *9*, 637.
- [32] B. H. Kim, M. S. Onses, J. B. Lim, S. Nam, N. Oh, H. Kim, K. J. Yu, J. W. Lee, J. H. Kim, S. K. Kang, C. H. Lee, J. Lee, J. H. Shin, N. H. Kim, C. Leal, M. Shim, J. A. Rogers, *Nano Lett.* **2015**, *15*, 969.
- [33] H. Li, Y. Duan, Z. Shao, G. Zhang, H. Li, Y. A. Huang, Z. Yin, *Adv. Mater. Technol.* **2020**, *5*, 2000401.
- [34] H. Wang, Y. Zhang, Y. Liu, Z. Chen, Y. Li, X. Li, X. Xu, *Nanoscale Adv.* **2023**, *5*, 1183.
- [35] S. J. P. Kress, P. Richner, S. V. Jayanti, P. Galliker, D. K. Kim, D. Poulikakos, D. J. Norris, *Nano Lett.* **2014**, *14*, 5827.
- [36] S. J. P. Kress, F. V. Antolinez, P. Richner, S. V. Jayanti, D. K. Kim, F. Prins, A. Riedinger, M. P. C. Fischer, S. Meyer, K. M. McPeak, D. Poulikakos, D. J. Norris, *Nano Lett.* **2015**, *15*, 6267.
- [37] T. A. Cohen, D. Sharp, K. T. Kluherz, Y. Chen, C. Munley, R. T. Anderson, C. J. Swanson, J. J. De Yoreo, C. K. Luscombe, A. Majumdar, D. R. Gamelin, J. D. Mackenzie, *Nano Lett.* **2022**, *22*, 5681.
- [38] V. A. Vlaskin, C. J. Barrows, C. S. Erickson, D. R. Gamelin, *J. Am. Chem. Soc.* **2013**, *135*, 14380.
- [39] A. Marmur, *Langmuir* **2004**, *20*, 3517.
- [40] Y. Chen, A. Ryou, M. R. Friedfeld, T. Fryett, J. Whitehead, B. M. Cossairt, A. Majumdar, *Nano Lett.* **2018**, *18*, 6404.
- [41] P. Geiregat, G. Allan, Z. Hens, C. Delerue, *Phys. Rev. B* **2016**, *93*, 115416.
- [42] C.-Y. Huang, C. Zou, C. Mao, K. L. Corp, Y.-C. Yao, Y.-J. Lee, C. W. Schlenker, A. K. Y. Jen, L. Y. Lin, *ACS Photonics* **2017**, *4*, 2281.
- [43] J. Lim, Y.-S. Park, V. I. Klimov, *Nat. Mater.* **2018**, *17*, 42.
- [44] H. Jung, N. Ahn, V. I. Klimov, *Nat. Photon.* **2021**, *15*, 643.
- [45] K. M. Walsh, K. Pressler, M. J. Crane, D. R. Gamelin, *ACS Nano* **2022**, *16*, 2569.
- [46] M. C. De Siena, S. E. Creutz, A. Regan, P. Malinowski, Q. Jiang, K. T. Kluherz, G. Zhu, Z. Lin, J. J. De Yoreo, X. Xu, J.-H. Chu, D. R. Gamelin, *Nano Lett.* **2020**, *20*, 2100.
- [47] K. Pressler, T. J. Snoeren, K. M. Walsh, D. R. Gamelin, *Nano Lett.* **2023**, *23*, 1320.
- [48] T. J. Milstein, D. M. Kroupa, D. R. Gamelin, *Nano Lett.* **2018**, *18*, 3792.
- [49] H. A. Nguyen, D. Sharp, J. E. Fröch, Y.-Y. Cai, S. Wu, M. Monahan, C. Munley, A. Manna, A. Majumdar, C. R. Kagan, B. M. Cossairt, *ACS Appl. Mater. Interfaces* **2023**, *15*, 4294.
- [50] W. H. P. Pernice, C. Xiong, C. Schuck, H. X. Tang, *Appl. Phys. Lett.* **2012**, *100*, 091105.
- [51] I. W. Frank, M. Lončar, M. W. McCutcheon, P. B. Deotare, *Opt. Express* **2010**, *18*, 8705.
- [52] H. Hodaie, M.-A. Miri, M. Heinrich, D. N. Christodoulides, M. Khajavikhan, *Science* **2014**, *346*, 975.
- [53] S. Zhang, Z. Yong, Y. Zhang, S. He, *Sci. Rep.* **2016**, *6*, 24487.
- [54] W.-Q. Wei, A. He, B. Yang, Z.-H. Wang, J.-Z. Huang, D. Han, M. Ming, X. Guo, Y. Su, J.-J. Zhang, T. Wang, *Light Sci. Appl.* **2023**, *12*, 84.
- [55] C. U. Hail, C. Höller, K. Matsuzaki, P. Rohner, J. Renger, V. Sandoghdar, D. Poulikakos, H. Eghlidi, *Nat. Commun.* **2019**, *10*, 1880.
- [56] A. Manna, J. E. Fröch, J. Censer, S. Pumulo, A. W. Barnard, J.-H. Chu, X. Xu, A. Majumdar, *ACS Photonics* **2023**, *10*, 3242.
- [57] M. Barelli, C. Vidal, S. Fiorito, A. Myslovska, D. Cielecki, V. Aglieri, I. Moreels, R. Sapienza, F. Di Stasio, *ACS Photonics* **2023**, *10*, 1662.